Numerical investigation of kerosene single droplet ignition at high-altitude relight conditions

A. Giusti[a,*], M.P. Sitte[a], G. Borghesi[b], E. Mastorakos[a]

[a]*University of Cambridge, Department of Engineering, Cambridge CB2 1PZ, UK.*
[b]*Sandia National Laboratories, Combustion Research Facility, 7011 East Avenue, Livermore, CA 94550, USA.*

Abstract

In this study, the fundamental problem of the ignition of a kerosene single droplet in a quiescent medium at engine high-altitude relight conditions is investigated using numerical simulations. The main objective is to improve the understanding of ignition phenomena with a focus on the effect of droplet evaporation in determining the growth of the ignition kernel and flame establishment. Results show that when the droplet is fully immersed in a high temperature region, ignition occurs when the scalar dissipation rate associated with evaporation decreases enough to allow the initiation of a flame. The ignition time depends on the droplet diameter and the far field temperature, i.e. the position of the droplet with respect to the spark location. As the fuel is consumed, the flame is found to move closer to the droplet surface until the flame cannot sustain itself any more due to increasing scalar dissipation rates. Furthermore, results show that at very low temperatures typical of high-altitude relight conditions no flammable mixture is available

*Corresponding author:
   Email address:* `ag813@cam.ac.uk` (A. Giusti)

1

around the droplet. Therefore, the success of an ignition event mainly depends on the energy released by the spark and the rate at which this energy is diffused toward the droplet surface to enhance the evaporation rate and create a flammable mixture. The findings are analysed from the perspective of gas turbine applications.

1. Introduction

An important requirement for aviation gas turbines is the capability to safely reignite after a flameout during the flight. This problem, usually referred to as *high-altitude relight*, involves the *forced ignition* of a spray at low pressure and low temperature conditions. Assuring high-altitude relight is a strong constraint on the design choices of engine manufacturers that has an impact on the engine weight and even on the operating envelope of the entire airplane. For this reason, the problem of spray ignition at high-altitude relight conditions has gained increasing attention.

Compared to gaseous mixtures, the ignition process of spray flames is significantly more complex due to the different scales and phenomena introduced by the presence of liquid fuel droplets [1]. Different ignition modes can be distinguished depending on the scale of the flame relative to the droplet dimension. Droplet ignition implies the formation of a flame around the droplet, or in its wake region if convective transport is present, whereas spray ignition represents the appearance of a flame involving the entire spray with a characteristic dimension of the flame larger than the droplet size. The intermediate case is represented by droplet cluster ignition where a flame around

2

clouds of droplets is generated. In all these modes, ignition is preceded by the evaporation of fuel droplets and the formation of a flammable mixture followed by kernel initiation and flame growth and establishment. As also pointed out in the recent review by Mastorakos [1], fuel volatility, droplet size and degree of pre-evaporation are important factors that distinguish spray ignition from gaseous flame ignition [2].

Kernel formation and flame growth in turbulent spray flames has recently been investigated using Direct Numerical Simulations (DNS) [3, 4, 5, 6]. In all these studies the droplets were considered as Lagrangian particles with point source approximation and, therefore, the droplet scale fuel distribution was not accurately resolved. Nevertheless, very interesting phenomena can still be observed and insight into the mechanism of flame initiation and establishment can be gained. From all these studies it is clear that the ignition of spray flames is strongly affected by the characteristics of the spray and evaporation phenomena. As also discussed in Ref. [7], a key parameter is the fraction of fuel that has been evaporated which depends on the energy released by the spark and the diameter of the droplets in the spark region. A spray population with smaller diameter generally requires lower energy for ignition due to the faster evaporation. In some cases [6], it has been shown that the deposition of the spark energy is followed by the formation of single droplet flames that eventually merge to give rise to a flame at the spray level. The formation of stoichiometric mixture bridges between the droplets is also an important phenomenon for flame propagation and has received increasing attention [8]. It is important to point out that a successful kernel generation does not necessarily require the presence of flammable mixture at the spark

location. A spark located outside of the nominal flammable region may result in a successful kernel generation if enough energy is diffused to the flammable region to cause ignition there [9]. The timescales associated with evaporation and the local evaporative cooling play an important role for the success of the initial kernel formation, but also for the subsequent flame growth and insufficient evaporation (fuel starvation) may lead to flame extinction even if a kernel was generated successfully [1].

Droplet size and the degree of pre-evaporation can be even more important at high-altitude relight conditions where the low temperature results in a very slow evaporation process and, therefore, strongly affects the availability of fuel in the region of the spark. Once the flame has extinguished, the low temperature environment together with a poor atomization (due to lower air flow rates) may cause a significant decrease in the amount of fuel that has evaporated implying the need of a larger amount of spark energy to initiate the flame kernel and to produce a self-sustaining (propagating) flame [10]. Experiments in model combustors (e.g. [11, 10, 12, 13]), usually focused on the effects of spray parameters, such as droplet mean diameter, fuel type, air pressure and temperature, have shown that a small mean droplet diameter and high fuel volatility generally increase the capability of flame ignition and stabilization in the combustor. Furthermore, the formation of a stable flame in the whole combustor usually happens with a given delay, due to both evaporation, flame initiation and propagation [11].

The objective of this study is to improve the understanding of forced ignition at high-altitude relight conditions with emphasis on the role of evaporation in determining the growth of the initial kernel and flame establish-

ment. The fundamental case of kerosene single droplet ignition in a quiescent medium is considered and studied by means of numerical simulations with detailed chemistry and fuel modelled as a multicomponent surrogate. The use of a quiescent (or nearly quiescent) configuration allows us to avoid additional complications arising from convective and turbulent transport and, therefore, to focus on the effects of evaporation and diffusion in the droplet near field. Although this study directly investigates single droplet ignition, it could also be relevant for spray ignition. As previously pointed out, it has been observed that the formation of the initial kernel can proceed through the formation of flames at the droplet scale that develop into a spray flame. Therefore, the single droplet case might be useful to give further insight into the first stages of the kernel development also in the more general case of spray combustion. Furthermore, the detailed solution of the droplet near field can complement the DNS studies that do not resolve the field close to the droplet surface due to the point approximation for the droplets.

The paper is organized as follows. First, the case of droplet evaporation under low pressure and temperature conditions is investigated. Then, droplet ignition results are discussed. The case of a spark much larger than the droplet diameter is considered as representative of typical aero-engine ignition processes. The effect of droplet diameter and temperature in the spark region on the mixture formation and initiation of the flame is studied. The more fundamental case of a spark located in the vicinity of the droplet surface is also considered to highlight the role of energy diffusion and evaporation in determining conditions in the droplet near field favourable for ignition. Conclusions and recommendations for future work close the paper.

2. Methodology

The fundamental case of an isolated droplet in the absence of any convective motion other than Stefan flow has been considered. This canonical case has received a lot of interest in the literature [14, 15, 16] and is further investigated here in the context of forced ignition of kerosene droplet at high-altitude relight conditions. An ambient pressure equal to 0.3 bar was considered here as representative of high-altitude conditions with the lowest ambient temperature equal to 250 K. Chemical reactions were modelled using a detailed kinetic mechanism developed for kerosene by Dagaut and Cathonnet [17, 18] with 209 species and 1673 reversible reactions, and reaction rates recommended for 1 atm. According to this mechanism, the kerosene fuel consist of a surrogate of three components, with the following molar composition [17]: 74% n-decane (n-$C_{10}H_{22}$), 15% n-propylbenzene (PH-C_3H_7), and 11% n-propylcyclohexane (CY-C_9H_{18}).

The liquid droplet was modelled as a three-component fuel, replicating the kerosene surrogate composition considered in the chemical mechanism. The single droplet ignition behaviour was investigated using the code described and validated in Refs. [16, 15, 19], in which the unsteady transport equations of mass, energy and species in spherical coordinates are simultaneously solved for both the gaseous and liquid phases according to the algorithm described by Cho et al. [20]. Details regarding the implementation of the multi-component solver can be found in Ref. [16], whereas the interested reader is referred to Refs [15, 19] for more details on the code and the solution algorithm. Additional information about the equations can also be found in Ref. [20]. Properties of the three liquid components were modelled

as detailed in Ref. [16].

The case of a droplet suddenly immersed in hot air was considered here as representative of a spark much bigger than the droplet diameter. Considering that the typical dimension of a spark are few mm (or even cm) while the droplet diameter is generally below 0.1 mm, this assumption appears reasonable, at least as a first approximation. Values of the air temperature T_{air} in the range from 1300 to 2000 K have been investigated to simulate the behaviour of a droplet located both in the spark region (high T_{air}) and in the region surrounding the spark that is heated up by the diffusion of spark energy. A pure evaporation case at low temperatures $T_{\mathrm{air}} = 250$ K, typical for high-altitude relight conditions is also investigated. Simulation for pure evaporation cases were performed without activating the chemical source terms.

The diffusion of spark energy in the droplet near field and its effect on the evaporation and mixture field has also been investigated through an idealised case, where a heat source was placed at a given radial position r_{spark} measured from the centre of the droplet. Due to the assumption of spherical symmetry, this "spark" is effectively shell-shaped, engulfing the droplet. While this is not a realistic geometry, the investigation is useful from an academic perspective, since it allows to explore how thermal diffusion of spark energy can lead to ignition. The spark is modelled as a source term in the energy equation. In physical space this heat source has a Gaussian shape (as a function of the radius), centred on r_{spark} with a characteristic width $w_{\mathrm{spark}} = 2\sigma_{\mathrm{spark}}$ and a peak value E_{spark}. A constant spark source is applied after a given evaporation time t_1 for the duration τ_{spark}. These

7

simulations also help quantify the evaporation time τ_{evap} as a function of ambient conditions.

The same numerical set-up described in Ref. [16] was used in this work. The droplet and gas phase were discretised with 600 and 300 nodes respectively. Pure air at a given temperature was imposed at the far-field boundary (located at a distance $r/r_{d,0} = 100$, where r is the radial coordinate and $r_{d,0} = d_0/2$ is the initial droplet radius), whereas an initial diameter and temperature were assigned to the droplet. A droplet temperature equal to 300 K was used in all cases with exception of the simulation with $T_{\mathrm{air}} < 300$ K where the initial droplet temperature was set equal to the ambience temperature. Both the droplet and the gas phase were initialised with uniform temperature and composition. Exponential fitting was used to initialise the gas phase close to the droplet surface, in order to smooth out the transition from the droplet interface to the far-field conditions and, therefore, improve the convergence of the code in the first steps of the simulation.

In the presentation of the results, the *mixture fraction* will be used quite often to show the mixing behaviour in the droplet near field. Here, Bilger's definition of mixture fraction was used [16, 15]. The stoichiometric mixture fraction for the surrogate used here is $\xi_{\mathrm{st}} \approx 0.063$. Nominal lean and rich flammability limits for kerosene at standard conditions are $\xi_{\mathrm{lean}} \approx 0.0324$ and $\xi_{\mathrm{rich}} \approx 0.1934$ [21] respectively. Flammability limits are often used to define a flammability factor [2]. However, ignition of a non-premixed flame may also start outside of these nominal limits [2]. Therefore, in the present work nominal flammability limits will only be used as a qualitative indicator of regions with flammable mixture.

3. Results and Discussion

In the following, results obtained from single droplet computations are discussed. First, the case of pure evaporation without the presence of a spark is discussed. Then results of droplet ignition in hot air are presented. One case of a localised spark is also discussed to highlight the role of diffusion and evaporation in the droplet ignition.

3.1. Evaporating droplets

Droplet evaporation at temperatures representative of high-altitude re-light conditions is discussed to highlight the evaporation time scales and the characteristics of the field around the droplet in the absence of a spark. Figure 1 shows the time evolution of the mixture fraction in the droplet near field for two different cases. In the case with $T_{\text{air}} = 250$ K and a small droplet diameter (Fig. 1 left), the mixture fraction (equal to the fuel mass fraction in a non-reacting case) at the droplet surface $\xi_s \approx 0.001$ is much lower than the nominal lean flammable limit of kerosene $\xi_{\text{lean}} \approx 0.0324$ [21] for the entire droplet lifetime. Hence, no flammable mixture is present in the gaseous domain, which highlights that it is critical for a spark to have sufficient energy, size and duration to heat up the droplet and to enhance the evaporation rate in order to ignite the gaseous mixture successfully. The fact that a spark needs to provide additional energy to ignite a droplet mist compared to the equivalent case of a homogeneous gaseous mixture, due to the heat required for fuel evaporation, has been pointed out in previous work [22] and is, in general, also associated with an increase of the minimum ignition energy. Since ignition happens in the gaseous mixture, the fraction of fuel in vapour
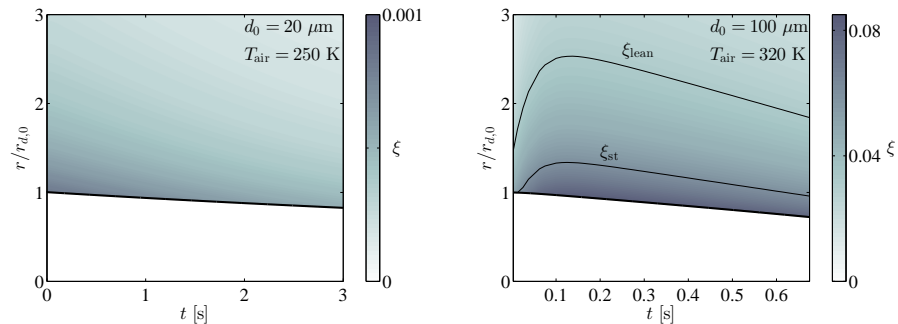
9

Figure 1: Temporal evolution of radial mixture fraction field in physical space, for $T_{\mathrm{air}} = 250$ K (left) and 320 K (right). The white area at the bottom represents the interior of the liquid droplet. The black line (only for $T_{\mathrm{air}} = 320$ K) mark the mixture fraction iso-lines at $\xi_{\mathrm{lean}} \approx 0.0324$ [21] and $\xi_{\mathrm{st}} \approx 0.063$.

form is an important factor for droplet and spray ignition.

It is instructive to compare this case with results from a simulation with higher gas temperature. Figure 1 (right) shows results from a case with $T_{\mathrm{air}} = 320$ K. This case can be representative of a scenario where after flame extinction in the combustor, a small amount of hot products mixed with fresh air is still present slightly enhancing the temperature of the mixture. Despite the small difference in temperature, the characteristics of the mixture around the droplet change drastically. As highlighted by the ξ_{lean} iso-line, a region with flammable mixture is present around the droplet, which extends over a radial distance of two initial droplet diameters. A mixture characterised by stoichiometric composition also appears very close to the droplet surface. It is interesting to analyse the extent of the region occupied by flammable mixture, which to some extent can be related to the ignition probability [2]. Due to the competing effects of evaporation and diffusion, the amount of flammable
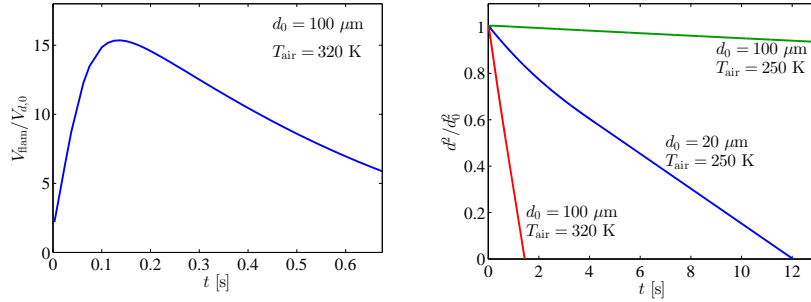
10

Figure 2: Time evolution of the volume of nominal flammable mixture normalised by the initial droplet volume for the case $d_0 = 100$ μm and T_{air}=320 K (left), and time evolution of the droplet diameter squared for selected cases (right).

mixture available in the gas phase changes in time. Figure 2 (left) shows the evolution of the volume of flammable mixture, based on nominal flammability limits, normalised by the initial droplet volume. At the beginning this volume increases rapidly, but then decreases due to the decrease of the evaporation rate (in kg/s) associated with smaller droplet diameters. Therefore, this plot shows that during the evaporation history of a droplet, it is possible to find a period where the availability of flammable mixture is maximum. This consideration could be very important in the case of a small spark located in the proximity of the droplet, whereas for a spark much bigger than the droplet diameter, the additional evaporation due to the hot region created by the spark itself will completely change this scenario.

Figure 2 (right) shows the time evolution of the droplet diameter squared for the two cases previously discusses. In addition the evaporation of a 100 μm droplet at 250 K is shown to emphasize the effect of the initial diameter. The variation in time of d^2 is almost linear showing that the d^2-law can be a good approximation of the droplet evaporation for almost the entire
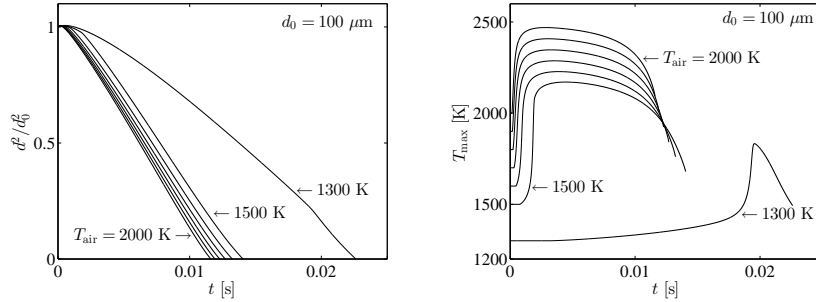
11

Figure 3: Temporal evolution of droplet diameter and maximum temperature of the gas phase for different air temperatures ($d_0 = 100\ \mu$m).

lifetime of the droplet. Furthermore, it is worth noting that the time required for the complete evaporation is of the order of 1 to 100 s depending on the initial gas-phase temperature and the droplet diameter. This time scale is much greater than the typical residence time in an aero-engine combustor. In absence of an external spark a significant part of the fuel is expected to exit the combustor in liquid form.

3.2. Single droplet ignition in hot air

A single droplet suddenly immersed in hot air can be a good approximation for cases characterized by a spark much bigger than the droplet diameter. In the following, the ignition behaviour for different values of the air temperature will be investigated. Furthermore, cases with different initial droplet diameter will be considered to highlight the role of the near-field mixing in the flame ignition and stabilisation.

Figure 3 shows the time evolution of the droplet diameter and maximum temperature of the gas phase for cases characterised by the same initial droplet diameter $d_0 = 100\ \mu$m but different air temperatures. Higher initial
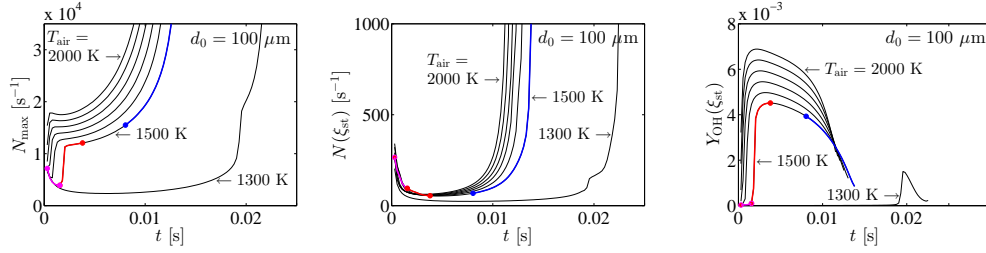
12

Figure 4: Temporal evolution of the maximum scalar dissipation rate (left) and the scalar dissipation rate (middle) and the OH mass fraction (right) at the stoichiometric mixture fraction. Coloured line elements are meant to help distinguish different phases in the ignition process

temperatures of the gas phase represent the cases of droplets located inside the spark, whereas cases with lower initial temperature may be representative of droplets located outside of the spark region, where the temperature increases due to the diffusion of spark energy. Ignition, detected as a sudden change of the maximum temperature in the gas phase, is observed for air temperatures greater than 1300 K. As also discussed in Ref. [16] for high pressure conditions, a higher gas temperature reduces the ignition delay time. A higher temperature decreases the time delay associated to evaporation and at the same time reduces the time scales associated to the chemistry determining a faster ignition. In the case with $T_{\mathrm{air}} = 1300$ K, the droplet ignition appears at the last stages of the droplet lifetime, when the droplet diameter is already quite small. A common feature of all the ignition events at high-altitude relight conditions, not observed in previous investigation of kerosene droplets at high pressure [16], is the strong decrease of the maximum temperature in the last stages of the droplet evolution.

This behaviour is explained through Fig. 4, which shows the maximum

13

value of the scalar dissipation rate N_{max} and its value at the stoichiometric mixture fraction $N(\xi_{st})$. The OH mass fraction at the stoichiometric mixture fraction is also shown. In the first part of the droplet lifetime, the scalar dissipation rate decreases (magenta line in Fig. 4). At the end of this period flame ignition occurs, which is highlighted by the increase of the OH mass fraction. At the same time the ignition also leads to a sudden rise of N_{max}, which can be attributed to the increase of droplet temperature and evaporation rate, leading to steeper mixture fraction gradients close to the droplet surface (red line). In contrast, $N(\xi_{st})$ still keeps decreasing until it reaches a minimum value. Eventually $N(\xi_{st})$ starts to increase (blue line) and the OH mass fraction as well as the peak temperature (Fig. 3 right) decrease as a consequence of finite-rate chemistry effects associated with faster mixing at the molecular level. Close to the complete evaporation, the scalar dissipation rate is too high to sustain a flame and the temperature drops down. However, complete extinction (i.e. absence of OH and heat release rate) is not observed before the complete evaporation. Another perspective on this ignition transient can be gained from the evolution of Y_{OH} and T in mixture fraction space (Fig. 5). At the beginning of ignition (blue profile), OH peaks at a very low $\xi < \xi_{st}$ highlighting the concept of the most reactive mixture fraction [2]. While stoichiometric and even very rich mixture up to $\xi \approx 0.8$ is still present at the last stages of the droplet lifetime (red profile), peak values of OH and temperature are low indicating that the flame approaches extinction through high scalar dissipation rates. It also interesting to note that close to the end of the droplet lifetime, when the scalar dissipation rate is high, the peak of both T and Y_{OH} moves towards leaner mixtures.
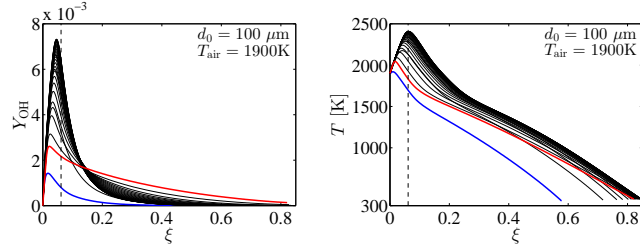
14

Figure 5: Mass fraction of OH (left) and temperature (right) as a function of mixture fraction. The blue and red line correspond to the instantaneous fields at $t = 2 \cdot 10^{-4}$ s and 0.0118 s respectively. The dashed black line marks the stoichiometric mixture fraction.
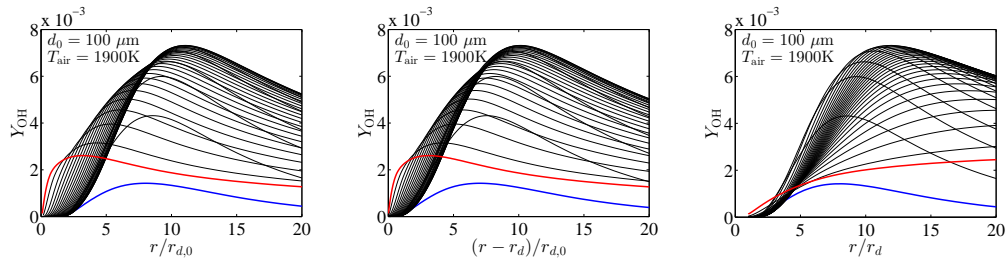

Figure 6: Ignition transient and flame location for the case $d_0 = 100$ μm, $T_{\mathrm{air}} = 1900$ K. The blue and red lines correspond to the start of ignition at $t = 2 \cdot 10^{-4}$ s and one of the last instances before extinction at $t = 0.0118$ s respectively.

An interesting quantity to be analysed is the location of the flame surface in physical space since it is directly influenced by both the combustion and evaporation processes. The flame location is visualized in Fig. 6 through the time evolution of OH mass fraction profiles as a function of different non-dimensional distances. In Fig. 6 (left), the Y_{OH}-profiles are plotted as a function of a non-dimensional radius defined as the ratio of the distance from the centre of the droplet r and the initial droplet radius $r_{d,0}$. This plot shows that the location of the flame in physical space, assumed here at the location of the peak of OH mass fraction, first moves to a slightly larger
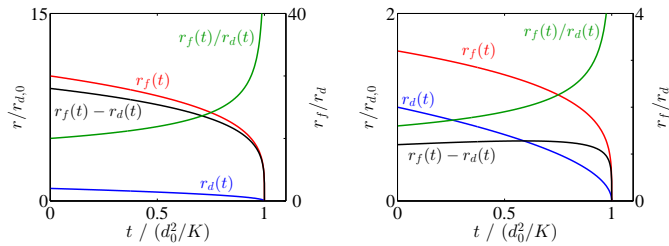
15

Figure 7: Theoretical analysis of the flame position for $r_{f,0}/r_{d,0} = 10$ (left) and $r_{f,0}/r_{d,0} = 1.6$ (right).

radius immediately after ignition and then moves back towards the droplet centre as the droplet further evaporates. The maximum radial distance of the peak of OH mass fraction is $r/r_{d,0} \approx 10$. Consistent with previous studies [23], this value is smaller than the typical flame location predicted by simplified theoretical models based on flame-sheet approximation and closer to experimental observations [23]. If the non-dimensional radius is computed using the instantaneous droplet radius r_d (i.e. the radius of the droplet at each time instant), the location of the peak moves to the right for the entire droplet lifetime (Fig. 6 right). This is consistent with previous studies [24], however it does not imply that the flame moves farther from the droplet surface as shown in Fig. 6 (middle), where the OH mass fraction profile is plotted as a function of the non-dimensional distance from the droplet surface $(r - r_d)$. This plot shows that the actual distance of the peak of OH mass fraction slightly increases immediately after the ignition event and then decreases until the droplet fully evaporates.

The movement of the flame towards the droplet surface long time after ignition can also be shown with an order of magnitude analysis. At constant properties for the liquid (this is a reasonable approximation after the droplet

16

heat-up period, although some deviations might be present due to the differential evaporation of the liquid components [16, 25]) and the gas phase, the well-known d^2-law [23] shows that the evaporation rate of the fuel $\dot{m}_f$ (in kg/s), is proportional to the instantaneous droplet diameter d whereas the evaporation rate per surface area is proportional to $1/d$.

$$\dot{m}_f \propto d, \qquad \frac{\dot{m}_f}{A_d} \propto \frac{1}{d} \tag{1}$$

Assuming the flame confined in a very thin region and neglecting the influence of the scalar dissipation rate on the chemical reaction, the heat release rate per unit area HRR (in $J/m^2/s$) is constant. At quasi-stationary conditions for the gas phase (at low pressure, this is a good approximation [14]), the droplet scale flame consumes all the fuel that is evaporated, leading to the energy balance,

$$\text{LHV } \dot{m}_f = \text{HRR } A_f \tag{2}$$

where LHV (in J/kg) is the lower heat value of the fuel and A_f is the surface of the flame. Assuming a spherical flame around the droplet (a reasonable assumption in the absence of convective and turbulent transport), $A_f \propto d_f^2$, hence Eq. 2 leads to

$$d_f^2 \propto d \tag{3}$$

Noting that $d_f > d$ is a necessary condition, and using the d^2-law,

$$d(t) = \sqrt{d_0^2 - Kt} \tag{4}$$

the location of the flame, $r_f = d_f/2$, and the droplet radius as a function of time can be plotted, as shown in Fig. 7. It is interesting to note that the distance of the flame from the droplet surface $(r_f - r_d)$ predicted by this analysis for $r_{f,0}/r_{d,0} = 10$ (Fig. 7, left) decreases in time meaning that the flame

17

moves closer to the droplet surface as the droplet evaporates. Furthermore, this analysis also suggests that for $r_{f,0}/r_{d,0} < 2$ the distance of the flame from the droplet surface, $r_f - r_d$, is characterized by an initial increase. Eventually, $r_f - r_d$ decreases to zero approaching the complete evaporation (Fig. 7, right). As previously mentioned, constant thermophysical properties for the droplet and the gas phase have been assumed in this analysis. Furthermore, finite-rate chemistry effects have not been considered.

Figure 8 (left) shows the temperature at the droplet surface (for several T_{air}). Sufficiently long after the initial heat-up period and the ignition, the temperature is relatively constant such that changes of the droplet properties are very small. The resulting evaporation rate (in kg/s) as a function of the droplet radius predicted by the numerical simulation is shown in Fig. 8 (right). Except for the case with $T_{\mathrm{air}} = 1300$ K where ignition happens at the last stages of the droplet lifetime and, therefore, a quasi-steady state is never reached, the other cases show a nearly linear dependence of the evaporation rate on the droplet diameter after the initial transient. The evaporation rate increases during the heat-up period and ignition transient (higher diameter) and then decreases proportionally as the droplet becomes smaller. The slight deviation from the linear behaviour might be related to small changes in the droplet temperature and composition and, more importantly, to changes of the gas-phase temperature that, as previously discussed, are significant (Fig. 3 right) especially close to the complete evaporation therefore determining changes in the structure of the droplet near field. Although the linear relation between the evaporation rate and the droplet diameter seems to be a good approximation sufficiently long after ignition, the de-
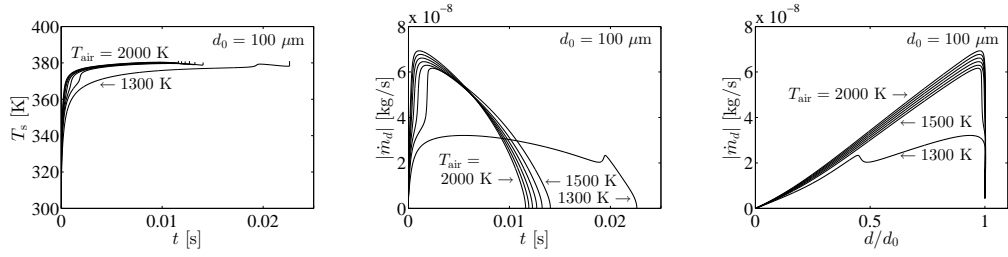
Figure 8: Time evolution of the temperature at the droplet surface (left) and evaporation mass flow rate as a function of time (middle) and droplet diameter (right) for the case $d_0 = 100$ μm.

pendence of the heat release rate on the scalar dissipation rate should also be considered. As discussed through Fig.4 (left), the scalar dissipation rate first decreases and then increases at the last stages of the droplet lifetime. An increase of scalar dissipation rate, far from extinction, generally corresponds to an increase of the local heat release rate. Therefore, for a given evaporation rate, it is expected that an increase of the scalar dissipation rate (and therefore heat-release rate) induces a movement of the flame towards smaller radii (Eq. 2). This behaviour supports the movement of the flame location towards the droplet surface long time after ignition when the scalar dissipation rate increases, whereas the initial movement of the flame to larger radii might be related to both the initial transient phenomena and the slight decrease of the scalar dissipation rate immediately after ignition.

Sufficiently long after ignition, when a diffusion flame around the droplet stabilises (far from extinction), the location of the flame can also be revealed by the location of the stoichiometric mixture fraction. This is shown in Fig. 9. The location of the stoichiometric mixture first moves to higher radii and then close to the droplet centre following the behaviour previously discussed

19

through the peak of OH mass fraction. Considering that the temperature at the droplet surface after the initial heat-up transient is nearly constant, the mixture fraction at the droplet surface varies only very little during the later stages of the droplet lifetime. The movement of the stoichiometric mixture fraction closer to the droplet surface further enhances the mixture fraction gradient $\partial \xi / \partial r$ and, therefore the scalar dissipation rate increases. In the same figure the iso-line of ξ_{lean} is also reported. Its distance from the droplet centre first increases and then decreases following the decrease of the evaporation rate (proportional to the droplet diameter, as previously discussed). Considering an array of droplets at fixed positions, the location of the flammable mixture gives to some extent (in this analysis the inter-droplet interactions are neglected) the critical distance between the droplets to form bridges, a phenomenon that has been identified as one of the possible mechanisms for the formation of a stable kernel and propagation of the flame in spray ignition [6]. The distance is maximum at intermediate stages of the droplet lifetime, when the scalar dissipation rate is almost constant, and this configuration might be identified as the most favourable for the formation of flame bridges between the droplet. This should be further investigated in future work. Finally, close to the droplet surface, very rich mixture is formed, beyond the nominal rich flammable limit.

The effect of the initial droplet diameter is shown in Fig. 10 for the case with $T_{\text{air}} = 1900$ K. For the diameters investigated here, the ignition time delay decreases with the droplet diameter. Smaller droplets are in general more difficult to be ignited. This can be related to the higher scalar dissipation rate and it is also highlighted by the lower peak value of the temperature. As
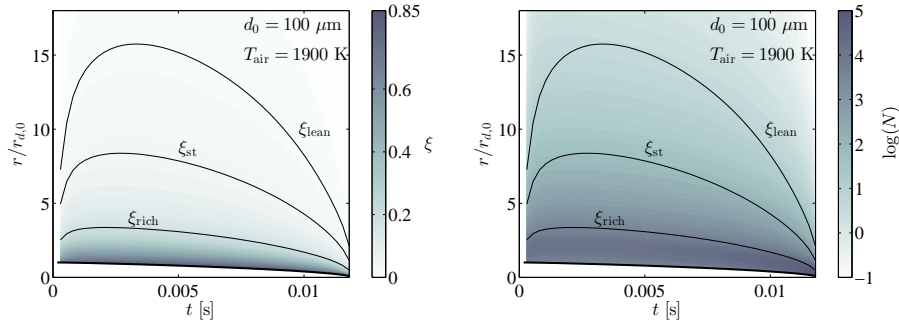
Figure 9: Location of the stoichiometric mixture fraction and nominal flammable limits as a function of time for the case $d_0 = 100$ μm, $T_{\mathrm{air}} = 1900$ K. Line plots have been superimposed to the mixture fraction (left) and scalar dissipation rate (right) fields.

the diameter is further decreased, the scalar dissipation rate increases until no ignition appears. Close to the critical droplet diameter, it is generally possible to find a value of the initial diameter for which the ignition delay is minimum. The existence of a optimal diameter for which the ignition delay is minimum has been extensively reviewed in Ref. [14] and has not been further investigated in this work.

3.3. Spark in the droplet near field

As previously discussed, the low temperatures that usually characterise high-altitude relight conditions do not allow the formation of flammable mixture around the droplet. Therefore, the spark should provide enough energy to increase the droplet temperature, enhance evaporation rate and then ignite the mixture. In order to show the effect of a spark on the generation of flammable mixture around the droplet, a pure evaporating case with a "spark" applied in the droplet near field was simulated. The case $d_0 = 20$ μm and $T_{\mathrm{air}} = 250$ K, previously discussed in the absence of a spark (e.g. Fig.1,
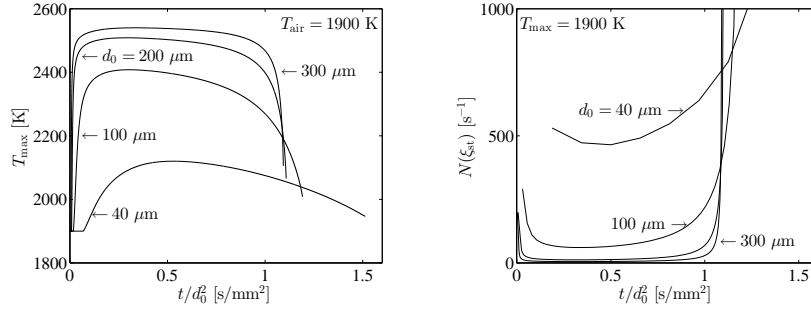
21

Figure 10: Temporal evolution of the maximum temperature of the gas phase and scalar dissipation rate at the stoichiometric mixture fraction for $T_{air} = 1900$ K and different initial diameters.

left), is considered again. An idealised spark located at $r_{spark} = 0.15$ mm with a width $w_{spark} = 0.05$ mm, peak energy $E_{spark} = 2 \cdot 10^{10}$ J/m^3/s and duration $\tau_{spark} = 0.1$ ms was applied after $t_1 = 0.6$ s. The time evolution of temperature and mixture fraction profiles in the droplet near field is shown in Fig. 11. The energy released by the spark causes a sudden increase of the temperature heating up the droplet and, thus, increasing the evaporation rate. A flammable mixture appears around the droplet, which extends for more than seven diameters in the radial direction, whereas close to the droplet surface very rich mixture is present with $\xi > \xi_{rich}$. The maximum distance of the nominal lean flammability limit ξ_{lean} from the centre of the droplet is reached at the end of the spark, then the diffusion and the absence of the spark energy causes a decrease of mixture fraction until after 3 ms no mixture inside the nominal flammability limits appears again. Ignition cases will be extensively studied in future work.
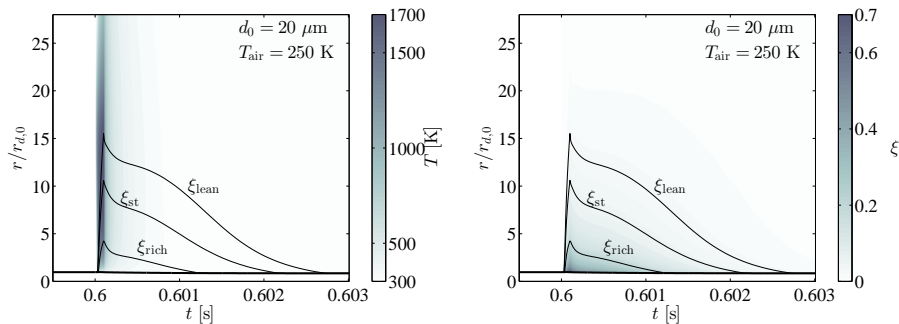
22

Figure 11: Location of the stoichiometric mixture fraction and nominal lean and rich flammable limits as a function of time for the case $d_0 = 20$ μm, and $T_{air} = 250$ K with spark applied. Line plots have been superimposed to the temperature (left) and mixture fraction (right) fields.

4. Conclusions

Kerosene single droplet ignition in a low pressure environment has been investigated using numerical simulations with the main aim of improving the understanding of ignition phenomena at high-altitude relight conditions.

The mixing field close to the droplet surface in the case of evaporation and ignition was studied, placing an emphasis on the role of evaporation in determining the location of the flame and the availability of flammable mixture in the gaseous phase. Results show that at temperatures typical for high-altitude relight conditions a spark is necessary to create flammable mixture around the droplet. In the case of a spark much bigger than the droplet diameter, ignition generally requires a sufficiently low scalar dissipation rate. The ignition time depends on the droplet diameter and the far field temperature, i.e. the position of the droplet with respect to the spark location. Furthermore, the location of the nominal lean flammable limit has

23

been observed to move far from the droplet immediately after ignition and then to move back toward the droplet surface in the last stages of the droplet lifetime. The location of the flammable mixture can be important for the creation of bridges between droplets and the transition to cloud combustion. The analysis proposed in this work can be extended to a wide range of conditions and initial droplet diameters to gain further insight into droplet ignition at engine relevant conditions. This will be attempted in future work.

5. Acknowledgement

References

[1] E. Mastorakos, Proc. Combust. Inst. 36 (2017) 2367 – 2383.

[2] E. Mastorakos, Prog. Energy Combust. Sci. 35 (2009) 57 – 97. doi:http://dx.doi.org/10.1016/j.pecs.2008.07.002.

[3] A. Wandel, N. Chakraborty, E. Mastorakos, Proc. Combust. Inst. 32 (2009) 2283–2290.

[4] A. P. Wandel, Combust. Flame 161 (2014) 2579 – 2600.

[5] A. Neophytou, E. Mastorakos, R. S. Cant, Combust. Flame 157 (2010) 1071 – 1086.

[6] A. Neophytou, E. Mastorakos, R. S. Cant, Combust. Flame 159 (2012) 641 – 664.

[7] S. Aggarwal, Prog. Energy Combust. Sci. 24 (1998) 565 – 600.

[8] T. Niioka, Combust. Sci. Technol. 177 (2005) 1167–1182.

[9] S. Ahmed, R. Balachandran, T. Marchione, E. Mastorakos, Combust. Flame 151 (2007) 366 – 385.

[10] M. Majcherczyk, N. Zarzalis, F. Turrini, Proc. ASME Turbo Expo (2014) ASME Paper GT2014–25332.

[11] D. W. Naegeli, L. G. Dodge, Combust. Sci. Technol. 80 (1991) 165–184.

[12] Y. Levy, V. Sherbaum, V. Nadvany, Y. Nehkamkin, J. Propul. Power 22 (2006) 828–834.

[13] A. Mellor, Prog. Energy Combust. Sci. 6 (1980) 347 – 358.

[14] S. K. Aggarwal, Prog. Energy Combust. Sci. 45 (2014) 79 – 107. doi:http://dx.doi.org/10.1016/j.pecs.2014.05.002.

[15] G. Borghesi, E. Mastorakos, Combust. Flame 162 (2015) 2544 – 2560.

[16] A. Giusti, J. Sidey, G. Borghesi, E. Mastorakos, Combust. Flame 184 (2017) 101–116.

[17] P. Dagaut, M. Cathonnet, Prog. Energy Combust. Sci. 32 (2006) 48 – 92.

[18] P. Dagaut, Phys. Chem. Chem. Phys. 4 (2002) 2079 – 2094.

[19] G. Borghesi, E. Mastorakos, Flow Turbul. Combust. 96 (2016) 1107–1121.

[20] S. Cho, R. Yetter, F. Dryer, J. Comp. Phys. 102 (1992) 160 – 179.

[21] H. F. Coward, G. W. Jones, U.S. Bureau of Mines Bulletin 503 (1952).

P. 120.

[22] D. R. Ballal, A. H. Lefebvre, Proc. Combust. Inst. 18 (1981) 1737 1746.

[23] C. Law, Prog. Energy Combust. Sci. 8 (1982) 171 – 201.

[24] N. Shaygan, S. Prakash, Combust. Flame 102 (1995) 1 – 10.

[25] A. Stagni, L. Esclapez, P. Govindaraju, A. Cuoci, T. Faravelli, M. Ihme, Proc. Comb. Inst. 36 (2017) 2483 – 2491.